Untouchable and Cancelable Biometrics: Human Identification in Various Physiological States Using Radar-Based Heart Signals

Daniel Foronda-Pascual, Carmen Camara and Pedro Peris-Lopez

***Abstract*— Biometric data are extensively used in modern healthcare systems and is often transmitted over networks for various purposes, raising inherent privacy and security concerns. Wearable devices, smartphones, and Internet of Things (IoT) technologies are common sources of such data, which are susceptible to interception during transmission. To mitigate these risks, cancelable biometrics offer a promising solution by enabling secure and privacy-preserving identification. In this study, we propose a cancelable identification model based on contactless heart signals acquired via continuous-wave radar. The recorded signal, which reflects cardiac motion, is first transformed into a scalogram. Feature extraction is then performed using Convolutional Neural Networks (CNNs), comparing models trained via transfer learning with those trained solely on the dataset. Before classification, the extracted features are converted into cancelable templates using Gaussian Random Projection (GRP), and classification is performed using a Multilayer Perceptron (MLP). The proposed method demonstrates feasibility, achieving 91.20% accuracy across all scenarios in the dataset, which increases to 95.40% when focusing solely on the resting scenario. Additionally, CNNs trained exclusively on the dataset outperform pre-trained models using transfer learning in feature extraction performance.**

***Index Terms*— Biometrics, Cancelable, Privacy, Identification, Continuous-Wave Radar, Transfer Learning, Template protection, Gaussian Random Projection, Heart dynamics**

I. Introduction

In recent years, the use of physiological data in healthcare systems has grown significantly, driven by technological advancements and the need for greater precision and efficiency in medical services. These data are collected from various sources, including wearable devices, the Internet of Things (IoT), and smartphones, which capture information such as fingerprints, heart rate readings, sleep patterns, and other physiological indicators. Once collected, the data serve a wide range of purposes in healthcare, including user identification, remote patient monitoring, early disease detection, and personalized medical treatments.

More specifically, biometrics [1] refer to the measurement and analysis of unique biological characteristics of individuals, which are used to identify or authenticate their identity. There are several types of biometrics, including i) Physical biometrics: These are based on the distinctive physical characteristics of a person. Common examples include fingerprints, iris, facial recognition, hand geometry, vascular structure, as well as heart dynamics used in this study. ii) Behavioral biometrics: These focus on the behavioral patterns of a person. Examples include signature, voice, keyboard typing rhythm, or walking style. These biometric data are captured by specialized devices, such as fingerprint scanners, facial recognition cameras, photodetectors, ECG electrodes or continuous-wave radar, and offer a secure and efficient way to manage identity and access in the healthcare domain.

As an identification system, biometrics offer significant advantages compared to traditional methods based on passwords or identification cards. One of the key advantages lies in the inherent uniqueness of biometric characteristics, which significantly reduces the risk of fraud and identity theft. Additionally, biometrics are convenient and quick to use, as they do not require users to remember complex passwords or carry physical identification cards. However, biometric systems also present certain drawbacks. A common concern is the privacy and security of biometric data, as an individual's biometric information is unique and highly sensitive. There is a risk of biometric data being compromised or stolen, which could have serious consequences for individuals' privacy and security [2]. An approach to address this particular challenge is through Biometric Template Protection (BTP) schemes. These methods modify the original biometric template to generate an alternative representation in a protected feature space, preventing leakage of information about the original sample during the identification process. The comparison procedure is conducted in this secure domain, thus safeguarding the data throughout the entire recognition process. The ISO/IEC 24745:2022 standard [3] regulates how these schemes should be implemented. Within BTP schemes, there are two classes: biometric cryptosystems and cancelable methods. Cancelable methods involve the irreversible transformation of the original biometric data into a distorted or masked representation, called

Manuscript received May 31, 2024; This work was supported by grants TED2021-131681B-I00 (CIOMET) and PID2022-140126OB-I00 (CYCAD) from the Spanish Ministry of Science, Innovation and Universities, as well as by the INCIBE under the project VITAL-IoT in the context of the funds from the Recovery, Transformation, and Resilience Plan, financed by the European Union (Next Generation).

All the authors are working for the Department of Computer Science, Carlos III University of Madrid (uc3m), 28911 Leganés, Spain. (emails: daniel.foronda@uc3m.es, mariacarmen.camara@uc3m.es, pedro.peris@uc3m.es) (Corresponding author: Daniel Foronda-Pascual)

a cancelable template. This template preserves certain unique characteristics of the individual that allow for identification while simultaneously ensuring that the original information cannot be reconstructed or recovered. Biometric cancellation can be achieved through various methods, such as encryption, feature transformation, or the incorporation of random noise into the biometric data. Cancelable biometric templates must exhibit the following characteristics [4]:

1) **Diversity:** A cancelable biometric template should not be used for more than one application. Each template must be unique and specific to a particular function or application, ensuring that it cannot be indiscriminately used in different contexts.
2) **Reusability/Revocability:** In case of compromise of the cancelable biometric template, a new cancelable template can be issued to replace the compromised one.
3) **Non-invertibility:** The original biometric template cannot be recovered from the cancelable biometric template.
4) **Performance:** The performance of the cancelable biometric-based system should not degrade compared to that of a traditional biometric system.

In this article we adopt a cancellation method. By employing biometric cancellation, systems can safeguard user privacy while maintaining the ability to accurately identify individuals, thus mitigating the risk of theft or compromise of biometric data. Even if the cancelable template is accessed, it will not reveal useful information about the original biometric traits of the individual. This removes the need for key management, reducing the risk of key compromise. Additionally, cancellation methods, unlike biometric cryptography, allow for the creation of unique templates for different applications and provide revocability, thereby enhancing privacy without the need for complex cryptographic processes. This technique has also been studied to preserve the privacy of various biosignals, including fingerprints [5], iris patterns [6], and palmprints [7].

In the field of heart signals, cancelable identification methods have been developed using ECG [8]–[10]. However, this technology has the drawback of requiring physical contact to capture the signal, which makes the identification method less versatile and applicable. In contrast, cardiac motion can be captured without contact through Continuous-Wave radar, providing a unique identifier for each individual, thereby enabling identification [11]. Although some studies have explored the effectiveness of this method for identification, they remain limited, typically involving a small number of subjects in a single resting scenario, and none have incorporated cancellation techniques [12]. Therefore, the objective of this paper is to advance the development of identification methods using such cardiac signals by creating a more secure method through the integration of cancellation techniques and by studying the impact of physiological variability on its performance.

A. Background

This article specifically explores the use of cardiac signals captured by radar, which reflect subtle chest wall movements caused by each heartbeat. The heart consists of two upper chambers (atria) and two lower chambers (ventricles). The circulation of oxygenated blood throughout the body is facilitated by the contraction (systole) and relaxation (diastole) of these four chambers in different phases. Each cycle is unique, varying in terms of volume, shape, movement dynamics, and heart deformation. These stages can differ among individuals due to factors such as size, position, heart anatomy, and thoracic configuration, making this signal a biometric identifier similar to how it occurs with ECG. Clinical investigations have confirmed that no two individuals have identical patterns of cardiac blood circulation [13]. Measuring the chest displacement produced by the heartbeat is directly linked to the sphygmogram, which represents changes in blood pressure over time. Specifically, the change in volume (ΔV) and pressure (ΔP) within an artery are related by the volumetric elasticity coefficient E [11], expressed as:

$$E = \frac{\Delta P}{\Delta V} \tag{1}$$

The radar-captured signal corresponding to chest movement combines superimposed components of venous and ventricular pulses. Continuous-wave radar technology is used to detect these signals by emitting and receiving continuous electromagnetic waves. When these waves interact with the heart and surrounding tissues, they produce a frequency shift that can be analyzed to extract valuable cardiac information [14]. This frequency shift is caused by the Doppler Effect, a phenomenon that occurs when electromagnetic waves reflect off a moving surface—in this case, the chest wall. The heartbeat generates slight chest movements, causing variations in the frequency of the reflected wave that enable the radar to capture and analyze these subtle cardiac fluctuations. A continuous-wave radar system includes a transmitter that emits electromagnetic waves and a receiver that detects the reflected signals. The transmitter generally has a radar antenna focused on the target area, and a data acquisition system collects and digitizes the radar signals for further analysis. This non-contact method offers several advantages, such as enabling continuous identification, capturing a broader range of data with minimal effort from the user, and maintaining a higher level of hygiene compared to other methods like ECG. Additionally, this technology can monitor respiratory patterns alongside cardiac activity simultaneously. However, there are limitations: currently, limited data are available for in-depth studies on this technology, and the signals may be more vulnerable to noise interference caused by unwanted movements, such as body motion, which remains an active area of ongoing research [15], [16].

B. Paper contribution

This paper proposes a cancelable identification system based on heart signals acquired non-invasively using continuous-wave radar. After preprocessing the signals and isolating the components corresponding to heartbeats, these are transformed into images (scalograms). Convolutional Neural Networks (CNNs) are used to extract features from these images, which are then employed to generate cancelable templates using Gaussian Random Projection (GRP). Finally, a Multilayer Perceptron (MLP) is used to classify these templates and identify individuals. The application of this type of signal in

the healthcare field is still in its early stages, and both studies and publicly available datasets remain scarce.

The main contributions of this paper are as follows:

- We propose, for the first time, a cancelable identification system based on contactless cardiac signals captured through Continuous-Wave radar, addressing the limitations of traditional ECG-based methods that require physical contact.
- We introduce the integration of cancelable biometric template protection (GRP-based) into a contactless cardiac identification system, ensuring enhanced privacy and security of the biometric data.
- We conduct a study of physiological variability and its impact on the performance of the identification system across different scenarios, providing insights into the robustness of the proposed method throughout different situations.
- We evaluate and compare the performance of CNN models using transfer learning with models trained from scratch for feature extraction from scalograms that synthesize cardiac information.

II. Related work

In this section, we review the current scientific literature relevant to our topic, categorizing it into two parts. Firstly, we examine articles focusing on the identification of individuals, especially using cardiac signals. Secondly, we explore articles that employ cancellation methods for biometric identification.

A. Identification using cardiac signals

In the field of biometrics, several modalities have traditionally received special attention, such as fingerprints, iris, or face recognition [17]. In the domain of cardiac-based biometrics, the most extensively analyzed signal has been the electrocardiogram (ECG) [18], with notable and promising results since as early as 2001 [19]. Initially, ECG was used to obtain heart rate [20], but later its use expanded for diagnosis [21], [22] or identification [23]–[25]. Several studies have focused on enhancing ECG-based identification by leveraging machine learning and deep learning techniques. For instance, [26] proposed a cascaded CNN architecture to improve identification accuracy, reaching 94.3% accuracy. Furthermore, [27] utilized Long Short-Term Memory (LSTM) networks to capture the temporal dynamics of the ECG signal, demonstrating a high accuracy of 97.3% in a dataset with 290 subjects. Recent approaches have explored novel representations of ECG signals. For example, [28] transformed ECG data into heatmaps, referred to as the Elektrokardiomatrix, and processed them using a CNN with a single convolutional layer, achieving an accuracy of 99.53%. Additionally, [29] proposed a novel biometric authentication system based on ECG detection, called BAED. This system utilizes deep learning algorithms, including a CNN and LSTM network, and is evaluated on both on-person and off-person databases. The model outperformed prior state-of-the-art approaches, reaching 99.49% accuracy with 90 subjects. Finally, in [30], the ECG signal was converted into a scalogram. Features were then extracted using a CNN and classified with a Support Vector Classifier (SVC), achieving 99.21% accuracy.

In addition to traditional ECG-based identification, several studies have investigated the use of heart rate (HR) and heart rate variability (HRV) as complementary or standalone biometric traits. For instance, in [31] they developed a method for short-term ECG-based identification that minimizes the effect of heart rate on the biometric template, achieving robustness against HR variations. Similarly, in [32] they proposed a methodology that explicitly incorporates HR into the identification model using Gaussian Mixture Models and Hidden Markov Models (GMM-HMM), achieving high accuracy. Beyond HR, HRV has also been explored as a potential feature for identification. In [33], an accuracy of 82.22% was achieved using HRV for biometric recognition, which was later improved by optimizing feature selection with genetic algorithms [34].

However, one of the main disadvantages of ECG is that it requires physical contact with the body to form an electrical circuit with the heart in it [35]. This renders ECG less suitable for applications such as continuous identification or monitoring of heart activity in daily life or during sleep. Therefore, the use of radar for capturing cardiac signals can be particularly advantageous in certain applications. In this context, studies have employed various types of radar, such as Continuous-wave (CW) radar, Ultra-wideband (UWB) radar, and Frequency-modulated continuous wave (FMCW) radar. Among these, CW radar is most commonly used, likely due to its technical simplicity and low cost [36]. This radar can detect variations in chest movement [37], making it possible to isolate the heart signal. To further refine the cardiac signal and eliminate noise components, body movements, and respiration, some studies use a Butterworth filter [38]. However, in [39], the authors demonstrate that Wavelet Packet Decomposition (WPD) outperforms Bandpass filters and Peak detection in isolating respiratory and cardiac signals. Later, in [40], various methods for this purpose were compared, including WPD, among which Discrete Wavelet Transform (DWT) achieved the best results.

In 2017, a method for identification based on the cardiac signal extracted via CW radar was developed [41] based on fiduciary analysis of the signal, which aims to identify specific points in the cardiac cycle that serve as stable references. In [11], the signal was divided into individual heartbeats. After resampling the heartbeats to a fixed number of samples, they were classified. In [42], they transformed the signal into spectrograms, which were then classified using Deep Convolutional Neural Networks (DCNNs). The applications of CW radar also span other fields such as identification from respiratory signals [43], gait recognition [44], event recognition [45], emotion recognition [46], and multi-person spatial tracking [47]. Nevertheless, it remains a relatively recent technology whose applications have barely been developed.

B. Cancellation techniques for biometrics

Cancelable biometrics techniques [48] intentionally and repeatably distort biometric data through transformations. Such

distortion can be applied either in the signal domain or the feature domain, preserving certain unique individual characteristics for identification purposes while ensuring that the original information cannot be reconstructed or recovered. These techniques can be categorized into two types: i) transformation schemes, which involve applying transformations to biometric data using parameterized one-way functions by secret information s, and ii) salting schemes, which involve incorporating additional information to the original biometric data in a unique and specific manner for each user or application context.

Within transformation schemes, various types are found such as Geometric Transforms, Random Permutations, BioConvolving, Polynomial Transforms, Random Projections, Hill Cipher, Correlation Filters, or Bloom Filters [49]. Specifically, Random Projections reduce the dimensionality by mapping biometric information onto random subspaces. Different distributions, such as Gaussian or sparse, determine the elements of the projection matrix, impacting both security and computational complexity [50]. Various techniques leveraging Random Projections have been developed for this purpose, including BioHashing [51], Random Multispace Quantization [52], Multi-space Random Projections [53], User-dependent Multi-state Discretization [54], Sectored Random Projections [55], Random projections with vector translation [56] or Dynamic Random Projections [57].

In [58], a cancelable multi-biometric system for person recognition based on fingerprint and finger-vein biometrics is proposed. This system utilizes an enhanced partial discrete Fourier transform (EP-DFT) non-invertible transformation to provide template protection and revocability.

Among the different variants of Random Projection, one of the most common is Gaussian Random Projection (GRP). For example, in [59], GRP is used as a cancelable method to identify individuals based on their iris, achieving an average accuracy of 95.65%. In [60], this technique is applied to fingerprint images for the same purpose. Other examples include its application in facial recognition [61] and palmprint recognition [62].

While there has been significant research on cancelable identification methods using fingerprints, face, or iris, the literature based on heart signals is not as extensive. ECG-based recognition has been investigated, for instance, in [63], where an ECG-Hash is used for template generation. In [64] they proposed a cancelable ECG biometric recognition system using a generalized likelihood ratio test (GLRT) in the compressive sensing domain. This system demonstrates resistance to various attacks through a random row permutation revocation mechanism. In [65], Subspace Collapsing is used to project ECG signals into a lower-dimensional space to obtain cancelable templates using a procedure conceptually similar to GRP, as both rely on projecting features into lower-dimensional spaces. In [66], they use an encryption method based on a 3D chaotic logistic map to transform ECG features into secure and revocable templates. The 3D chaotic logistic map is a nonlinear dynamic system with chaotic behavior, meaning it is highly sensitive to initial conditions and generates pseudo-random sequences. These properties make it suitable for encryption purposes, as small changes in the input lead to significant and unpredictable changes in the output. In [67], using one-dimensional ECG and audio signals, a blind signal separation algorithm is employed to obtain distorted ECG signals that can be used as cancelable templates. However, to the best of our knowledge, no studies have yet explored the feasibility of a cancelable identification process using non-contact heart signals extracted via radar.

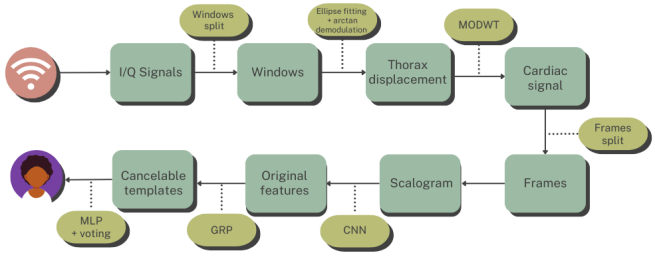

Fig. 1. Overview of the identification process

III. Materials and Methods

This section examines the dataset used, comprising cardiac signals from 30 patients across various physiological scenarios, and outlines the procedure used to develop a cancelable identification method based on these signals. As illustrated in Fig. 1, the procedure begins by dividing each patient's recording, lasting several minutes, into 10-second segments, which are subsequently used as input for the identification model. The goal is to identify which of the 30 patients each test window corresponds to. To achieve this, we first apply arctan demodulation and the Maximal Overlap Discrete Wavelet Transform (MODWT) method to extract the cardiac movement component from each 10-second window. This 10-second cardiac signal is then subdivided into 4-second frames as a form of data augmentation. For each frame, a scalogram is generated, and its features are extracted using a CNN. These features are then transformed into a cancelable template through the application of GRP. Finally, an MLP classifier categorizes these templates among the 30 patients, assigning a predicted patient to each frame. To assign a final prediction for the entire window, a majority vote is conducted, considering the predictions for all frames within the window. In this way, the model outputs the predicted patient for the full window.

A. Data

The research utilized a publicly accessible dataset [68] gathered at Erlangen University Hospital in Germany, comprising records from 30 individuals (14 men and 16 women) with an average age of 30.7 years, where a radar system captured chest movements in a contactless manner. These chest movements result from a combination of body movements, respiration, and heartbeat. The radar system used in the study was optimized for a distance of approximately 40 cm from the area of interest. Utilizing Six-Port technology, the system was designed for mobility and features a bi-static antenna setup with transmitting and receiving antennas set at $\pm 10^{\circ}$ angles and a laser for alignment purposes.

The measurements comprised five distinct scenarios: a resting scenario where participants reclined in a relaxed position for at least 10 minutes with calm breathing; a Valsalva maneuver scenario involving three repetitions of forceful expiration against a closed glottis for 20 seconds, with intervals of 5 minutes; an apnea scenario where participants held their breath after inhaling or exhaling completely, with raw signal recording during the transition to apnea; a tilt-up scenario where the tilt table was gradually raised from 0 degrees to 70 degrees to induce autonomic nervous system responses; and a tilt-down scenario starting from the 70 degrees tilt-up position, gradually lowering the table back to the starting horizontal position, with similar ANS reactions anticipated. The recordings in the Resting, Tilt-down, and Tilt-up scenarios lasted approximately 10 minutes. In the Apnea scenario, the duration was typically shorter, ranging from 2 to 8 minutes, while in the Valsalva scenario, the duration consistently exceeded 15 minutes. The dataset is accessible at [69].

B. Preprocessing

With the quadrature signals I/Q provided by the dataset, the first step is to segment these signals into temporal windows. The literature reports various window durations, ranging from a few seconds, such as 5 seconds in [70], 6 seconds in [42], and 10 seconds in [71], to longer intervals of 20 or 50 seconds [72]. In our study, we have selected a 10-second window to strike a balance between model efficiency and practical applicability. However, further investigation into how the size of this window influences the model's performance will be a topic for future research. Once we have segmented the recordings into 10-second windows, the next step is to demodulate the I/Q signal. Several methods for this process have been analyzed in [73], among which arctangent demodulation is one of the most commonly used [41], [74]. Therefore, we perform ellipse fitting on the I/Q points within each window, following the procedure outlined in [75], to carry out arctangent demodulation using the parameters obtained from the fitted ellipse [76]. The result of this process corresponds to the movement occurring in the region of interest (the thorax), which is composed of different components, with the main ones being the patient's movement, respiration, and cardiac motion. To isolate the latter, we apply the Maximal Overlap Discrete Wavelet Transform method (MODWT) following [77], where the method's performance is evaluated against alternative approaches yielding better results. Subsequently, the signal corresponding to the cardiac motion of each window is subdivided into frames to classify each frame, similar as in [11] is done with heartbeats. From the signal of each frame, we obtain its scalogram.

A scalogram is a visual representation of how the frequency components of a signal evolve over time [78]. It is obtained by applying a Continuous Wavelet Transform (CWT) to the signal, decomposing it into frequency components across time. Unlike a traditional time-domain or frequency-domain representation, the scalogram combines both time and frequency dimensions, showing how the frequencies change with respect to time. In this representation, the horizontal axis corresponds to time, and the vertical axis represents scales, which are inversely related to frequency—higher scales correspond to lower frequencies, while lower scales correspond to higher frequencies. Scalograms are particularly useful for analyzing non-stationary signals, such as cardiac signals, as they capture both temporal and frequency-based features that can be leveraged for classification tasks, like those performed with Convolutional Neural Networks (CNNs). In addition to the scalogram, several other techniques can transform a signal into an image for analysis with CNNs. The study in [79] compares the effectiveness of various methods for extracting signal features, including Gramian Angular Field, Markov Transition Field, Recurrence Plot, Grey Scale Encoding, Spectrogram, and Scalogram. Among these, the scalogram demonstrated the best performance though the authors also noted that the effectiveness of each method may vary based on the type of dataset used. While research on cardiac radar signals is limited, the scalogram has been widely and successfully applied in the field of ECG, particularly due to its robustness with noise-sensitive signals [80]–[84]. In our case, the scalograms are generated by applying the CWT to radar signals using the PyWavelets library. The Morlet wavelet, known for its good time-frequency localization properties, is chosen for its effectiveness in capturing frequency variations over time, especially in non-stationary signals [85]. In the resulting scalogram, the horizontal axis represents time, illustrating how the signal's frequency components evolve over time. The vertical axis corresponds to the frequency of the signal, typically ranging from 0 to 0.35 Hz, though it is represented in terms of scale due to the nature of the CWT.

For the segmentation of windows into training and testing sets, a specific percentage of the last windows in each patient's recording is selected as the test set (the last 20% of them), while the remaining windows constitute the training set. By selecting the last 20% of the windows from each patient for testing, we implement a temporal split. This approach more closely mirrors the real-world application of this system compared to a random split of the windows, as test samples are likely to be collected at temporally distant intervals, sometimes several months apart, from the training samples.

C. Feature extraction and Transfer Learning

Convolutional Neural Networks (CNNs) are nowadays one of the main methods for feature extraction in the field of computer vision [86]–[88]. Their hierarchical architecture, which mimics the visual cortex's organization in the human brain allows them to automatically learn meaningful representations from raw pixel data demonstrating exceptional performance across a wide range of visual tasks. Transfer learning [89], [90] can boost the performance of these networks by taking pre-trained models on large datasets like ImageNet [91] and fine-tuning them on specific tasks with different datasets. This approach not only accelerates the training process but also often leads to improved generalization performance, as the pre-trained model has already learned rich hierarchical features from vast amounts of data. Transfer learning has not only demonstrated great potential for real-world image

analysis but has also yielded strong results when processing signal-derived images, such as spectrograms and scalograms [92]–[97]. This makes it a relevant technique to consider for feature extraction, as it has proven effective in previous studies involving scalograms derived from other types of biosignals.

In this study, we tried feature extraction using five pre-trained networks: ResNet50 [98], DenseNet [99], ShuffleNet [100], VGG-19 [101], and Xception [102]. In these networks, we replace the last dense layers with others adapted to our problem, training only the parameters of these layers and freezing the rest [103]. The objective of transfer learning is to improve the performance and convergence speed on a target task with limited data often leading at the same time to better generalization. In addition to these networks, we used a customized CNN for feature extraction that was trained solely with the dataset scalograms. Its architecture, depicted in Figure 2, consists of five convolutional layers progressively increasing the depth of the representation. Following each convolutional layer, batch normalization [104] is applied, along with ReLU activation to introduce non-linearities, and max pooling. After the convolutional layers, the output is flattened and passed through two fully connected layers, serving as the final classifier, with the output processed through a LogSoftmax activation function. In Table I, the processing details of a batch of images with dimensions $3 \times 224 \times 224$ (channels $\times$ height $\times$ width) are outlined, where b represents the batch size, and *Param #* refers to the number of adjustable parameters associated with each layer of our CNN. The adjustable parameters in a neural network are the values that the network learns during the training process to minimize the prediction error. These include the weights of the connections between neurons and the biases associated with each neuron. In a convolutional layer (Conv2d), the weights correspond to the filters applied to the input, and the bias is a value added to the result of the convolution. In a batch normalization layer (BatchNorm2d), the adjustable parameters are the scale and shift factors used to normalize the data. In fully connected layers (Linear), the adjustable parameters are the weights of the connections between input and output neurons, along with the biases. Activation layers such as ReLU and pooling layers like MaxPool2d do not have adjustable parameters, as they only modify the data without learning a value.

TABLE I
STRUCTURE OF THE CUSTOMIZED CNN

Layer (type)	Output Shape	Param #
Conv2d-1	[b, 16, 220, 220]	1,216
BatchNorm2d-2	[b, 16, 220, 220]	32
ReLU-3	[b, 16, 220, 220]	0
MaxPool2d-4	[b, 16, 109, 109]	0
Conv2d-5	[b, 64, 107, 107]	9,280
BatchNorm2d-6	[b, 64, 107, 107]	128
ReLU-7	[b, 64, 107, 107]	0
MaxPool2d-8	[b, 64, 53, 53]	0
Conv2d-9	[b, 128, 41, 41]	1,384,576
BatchNorm2d-10	[b, 128, 41, 41]	256
ReLU-11	[b, 128, 41, 41]	0
MaxPool2d-12	[b, 128, 20, 20]	0
Conv2d-13	[b, 256, 16, 16]	819,456
BatchNorm2d-14	[b, 256, 16, 16]	512
ReLU-15	[b, 256, 16, 16]	0
MaxPool2d-16	[b, 256, 8, 8]	0
Conv2d-17	[b, 512, 7, 7]	524,800
BatchNorm2d-18	[b, 512, 7, 7]	1,024
ReLU-19	[b, 512, 7, 7]	0
MaxPool2d-20	[b, 512, 4, 4]	0
Linear-21	[b, 1024]	8,389,632
ReLU-22	[b, 1024]	0
Dropout-23	[b, 1024]	0
Linear-24	[b, 30]	30,750
LogSoftmax-25	[b, 30]	0

D. Cancellation and classification

Once feature extraction has been performed on each scalogram, we apply a cancellation technique. In this study, Gaussian Random Projection (GRP) [105] is employed for this purpose. GRP facilitates the projection of high-dimensional biometric feature vectors onto lower-dimensional spaces using randomly generated Gaussian matrices, thereby preserving the discriminative information essential for biometric identification. Random projections have the effect of reducing the dimensionality of the data. If we let N denote the number of samples and M denote the number of features extracted from each sample, by multiplying the feature matrix $\mathbf{X} \in \mathbb{R}^{N \times M}$ by a matrix $\mathbf{A} \in \mathbb{R}^{M \times m}$ whose elements follow a certain probability distribution, such as the Gaussian distribution, we obtain a new feature matrix $\mathbf{Y} \in \mathbb{R}^{N \times m}$ with $m < M$. This operation can be mathematically expressed as:

$$\mathbf{Y} = \mathbf{X} \cdot \mathbf{A} \tag{2}$$

where $\mathbf{Y}$ is the resulting feature matrix, $\mathbf{X}$ is the original feature matrix, and $\mathbf{A}$ is the random projection matrix.

Through the Johnson-Lindenstrauss lemma [106], we know that when performing this projection, the relative distances between any pair of points are approximately preserved in the new feature space following the next rule.

Johnson-Lindenstrauss lemma: For any $0 < \varepsilon < 1$ and any integer n, let m be a positive integer such that $m \geq m_0 = O(\varepsilon^{-2} \log n)$. For any set S of n points in $\mathbb{R}^N$, there exists a map $f : \mathbb{R}^N \to \mathbb{R}^m$ such that, for all $u, v \in S$:

$$(1-\varepsilon)\|u-v\|^2 \leq \|f(u)-f(v)\|^2 \leq (1+\varepsilon)\|u-v\|^2 \tag{3}$$

where $||.||$ denotes the vector 2-norm. Thanks to the approximate preservation of these distances in the new feature space, effective classification of the samples is possible, thereby enabling the identification of the corresponding subject for each one [107].

An influential parameter in the GRP process is ϵ, which regulates the quality of dimensionality reduction. Its significance lies in determining the degree of orthogonality among the randomly generated projection vectors. A lower ϵ value results in more precise projections, ensuring that the projected vectors closely approximate orthogonality. However, achieving this higher precision often comes at the cost of increased computational complexity. Conversely, a higher ϵ value expedites computation but may compromise precision, as the projected vectors deviate further from strict orthogonality.

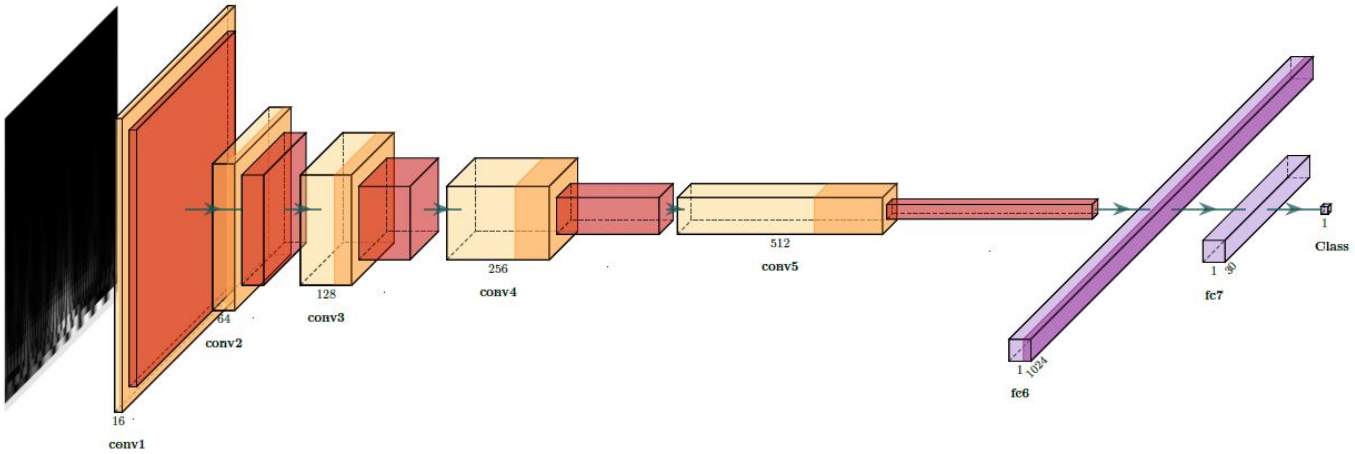

Fig. 2. Structure of the customized CNN (graph)

Finally, we employ a Multilayer Perceptron (MLP) to classify the cancelable template of each frame. Its architecture consists of three hidden layers with 1024, 256, and 64 neurons, respectively, each utilizing the ReLU activation function to introduce non-linearity. To prevent overfitting, a dropout rate of 0.2 is applied after each hidden layer. The model is trained using the Adam optimizer with a learning rate of 0.001 and a batch size of 1024. The number of training epochs is dynamically determined through early stopping, ceasing training if the validation performance does not improve for 10 consecutive epochs. After obtaining frame-level predictions with the MLP, the final class for each window is determined by majority voting across the predictions of its constituent frames.

IV. Results

In this section, we examine the different experiments conducted to develop a cancelable identification method, as well as the results obtained. First, we performed a comparison of several CNN architectures to determine which one extracts features from the scalograms more efficiently. To this end, we compared multiple CNN architectures initialized with pre-trained weights from the ImageNet-1K (v1) dataset [108], utilizing transfer learning, with a custom CNN trained solely on the scalograms from the training set. The latter provided better results. Additionally, when converting the features extracted from the scalograms by the CNN into cancelable templates, a key parameter is the amount of dimensionality reduction applied. In Subsection C, we analyze how this parameter influences the model's performance. Finally, in Section D, we study the identification results across each of the five scenarios, achieving an accuracy of 95.40% in the Resting scenario.

A. Metrics

When assessing the efficiency of the identification process, we will utilize various metrics, with accuracy being the primary one due to its reliable reflection of the model's performance when classes are balanced. Accuracy is defined as:

$$\text{Accuracy} = \frac{\text{Number of correctly identified samples}}{\text{Total number of samples}} \tag{4}$$

Additionally, we will consider other metrics such as False Acceptance Rate (FAR), False Rejection Rate (FRR), precision, recall and F1-score, defined in terms of False Positives (FP), True Positives (TP), False Negatives (FN), and True Negatives (TN) [109]. FAR measures the rate at which the system incorrectly identifies an unauthorized user as being authorized:

$$\text{FAR} = \frac{FP}{FP + TN} \tag{5}$$

FRR reflects the rate at which the system incorrectly rejects an authorized user:

$$\text{FRR} = \frac{FN}{FN + TP} \tag{6}$$

Precision represents the ratio of correctly identified positive cases to the total number of cases identified as positive:

$$\text{Precision} = \frac{TP}{TP + FP} \tag{7}$$

Recall measures the ratio of correctly identified positive cases to the total number of actual positive cases:

$$\text{Recall} = \frac{TP}{TP + FN} \tag{8}$$

and F1-Score, which is the harmonic mean of precision and recall, offers a balanced assessment of the model's performance, especially when there is an imbalance between classes:

$$\text{F1-Score} = 2 \times \frac{\text{Precision} \times \text{Recall}}{\text{Precision} + \text{Recall}} \tag{9}$$

B. Feature extraction evaluation and analysis

To evaluate how effectively each network extracts features, we performed the classification on a validation set using an MLP, based on features extracted by each network without the use of cancellation templates. The results are presented in Table II, reflecting both the accuracy in predicting the patient

TABLE II
ACCURACY IN CLASSIFICATION USING DIFFERENT NETWORKS FOR FEATURE EXTRACTION

	All scenarios		Resting scenario	
Network	**Windows acc.**	**Frames acc.**	**Windows acc.**	**Frames acc.**
ResNet50	88.32	77.88	93.09	87.92
VGG-19	85.88	77.72	89.51	84.57
Xception	85.15	74.36	92.07	85.70
DenseNet	84.35	71.00	91.30	82.54
ShuffleNet	80.22	67.72	87.72	75.34
Customized CNN	89.46	80.87	96.16	91.09

for the 10-second windows and for the 4-second frames into which these windows are subdivided.

These results show that feature extraction, both in the Resting scenario and in the combined set, is performed more effectively by our customized CNN, which was not pre-trained on other images and therefore does not use transfer learning. Among the pre-trained networks we used, ResNet50 performs the best. This outcome may be partly due to the difference between the images in our dataset and those in ImageNet, on which ResNet50 was originally trained. More importantly, it may suggest that the type of feature extraction needed to classify our images differs fundamentally from the feature extraction required to recognize objects in natural images. This suggests a potential domain mismatch [110]. In any case, for the remainder of the study, we considered only our customized CNN for feature extraction unless otherwise specified.

In addition, to gain a deeper understanding of the mechanisms underlying our CNN and how it identifies patients from scalograms, we conducted an analysis of the activation patterns generated by the network. For this purpose, we utilized the Convolutional Block Attention Module (CBAM), introduced in [111], which has previously been applied to study interpretability in the analysis of other biosignals, such as ECG [112]–[114]. This approach is in line with the principles of Explainable Artificial Intelligence (XAI) described in [115], which emphasize the importance of ensuring transparency in AI models and enabling human understanding of the reasoning behind decisions, particularly in high-stakes applications like healthcare. CBAM is an attention mechanism designed to enhance the performance of convolutional neural networks by enabling them to focus on the most relevant features of the input data. This mechanism is applied sequentially in two stages: channel attention and spatial attention. Channel attention assigns a weight to each feature channel, helping the model identify the most informative channels for the task. On the other hand, spatial attention assigns weights to specific spatial locations within each feature map, helping the model focus on the most relevant regions within the image or signal. These complementary mechanisms enhance performance and interpretability by helping the network prioritize the features and regions that most influence its decisions. In our case, we incorporated the CBAM module following the RELU-15 layer (see Table I) and retrained the CNN. The inputs to the module consist of 256 feature maps of size 16 x 16, to which a 3 x 3 kernel is applied. In Figure 3, we present six randomly selected scalograms alongside their

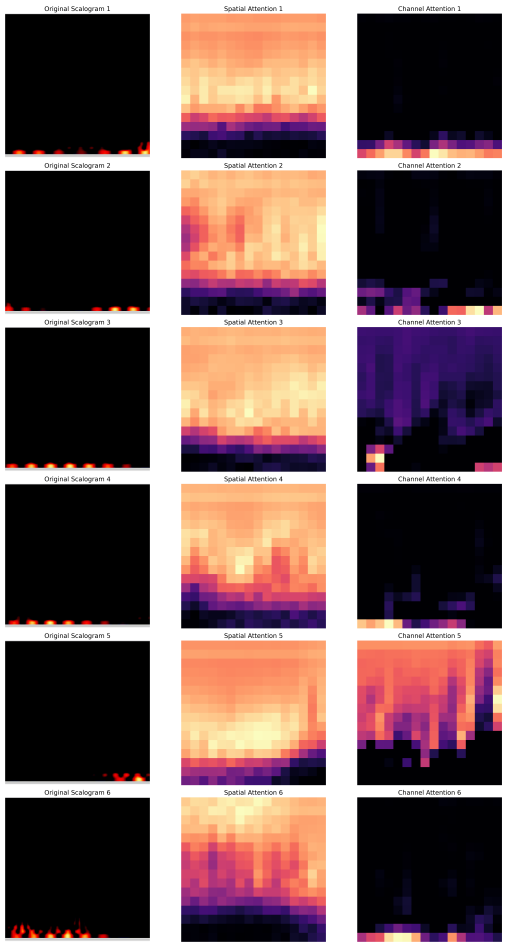

Fig. 3. Randomly selected scalograms (left), corresponding spatial attention map (center), and channel with highest attention (right)

corresponding spatial attention maps and the feature map exhibiting the highest channel attention. It is worth noting that the visualization of the original scalograms (with time on the horizontal axis and frequency on the vertical axis) is not particularly intuitive for the human eye, as the presence of high values in the lower frequencies (at the bottom) obscures more subtle yet important differences in the higher frequencies. However, as observed in the central column, the CBAM consistently places greater attention on mid-to-high frequencies, potentially because these regions contain the most discriminative information for distinguishing between subjects. In the right column, we present the feature map exhibiting the highest attention for each scalogram, where, in certain cases, regions corresponding to high and mid frequencies are also accentuated. While further detailed and comprehensive analysis is needed to draw definitive conclusions, these initial findings suggest that these frequency regions may play a crucial role in patient identification within each scalogram. This observation suggests the need for further investigation and provides a potential direction for research.

C. GRP and dimensionality reduction

By randomly projecting the data onto a lower-dimensional subspace defined by Gaussian distributions, GRP effectively

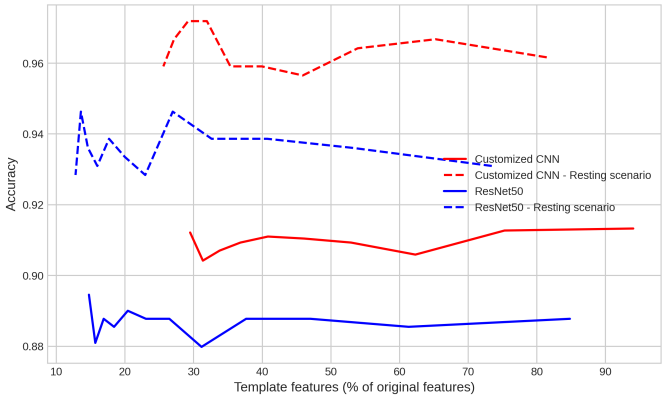

Fig. 4. Accuracy vs. Strength of dimensionality reduction in GRP

compresses the data representation. The parameter ϵ governs the degree of compression, with smaller values leading to less aggressive reduction and higher-dimensional projections, while larger values result in more compact representations. We conducted a comparative analysis of dimensionality reduction effectiveness as a function of the GRP parameter ϵ, in relation to the resulting accuracy. Figure 4 illustrates this in two different contexts: identification in any scenario and identification in the Resting scenario. The x-axis shows the percentage obtained by dividing the number of features in the cancelable templates by the number of original features from the CNN. It can be seen that accuracy exhibits a seemingly indifferent response to varying degrees of dimensionality reduction.

Concerning scenarios, as expected, outcomes within the Resting scenario outperform those of all scenarios, likely due to its inherent homogeneity compared to settings involving disturbances such as tilt variation or apnea. The figure also confirms that using a customized CNN for feature extraction yields better performance than transfer learning.

D. Identification

Finally, we analyze the efficiency of patient identification using the complete model. Initially, we extract features with both ResNet50 and our customized CNN and apply GRP to generate cancelable templates with $\epsilon = 0.6$. As previously mentioned, the train-test split was done temporally. Using a random split would have yielded notably higher accuracy but would not reflect a realistic real-world scenario. When breaking down the predictions by scenario, as illustrated in Table III, we can observe that the results obtained by extracting features with our CNN are superior across all scenarios. We can also observe that the most challenging scenarios to predict are Apnea and Tilt Up, while the results for the other scenarios exceed 90% accuracy. The difficulty in the Tilt Up scenario might be partly due to the significant effort required by the heart as the body moves from a horizontal to a vertical position, given that the organs with the highest blood demand are located in the upper part of the body. For the Apnea scenario, the recordings are shorter than in the other scenarios, with only three apneas per recording, which may result in insufficient training data for effective generalization, also considering that apneas can be of two different types: after inhaling or after exhaling. Table IV provides a more detailed overview of the metrics obtained during the classification process, both in the Resting scenario and across all scenarios.

TABLE III
ACCURACY OF THE MODEL IN DIFFERENT SCENARIOS USING RESNET50 AND CUSTOMIZED CNN FOR FEATURE EXTRACTION

Scenario	ResNet50	Customized CNN
Apnea	70.71	74.75
Resting	93.86	95.40
TiltDown	93.54	95.51
TiltUp	73.65	78.19
Valsalva	94.69	94.87

Furthermore, predicting the class of each window by voting over its frames allows us to obtain a confidence measure. That is, each window w is decomposed into a set of frames $\{f_i^w \mid i \in \{1, 2, ..., k\}\}$. For each frame f_i^w, the model provides a prediction of which class it belongs to, $c(f_i^w)$, and the predicted class of the window is the mode of the predictions of its frames:

$$c(w) = mode(c(f_1^w), c(f_2^w), ..., c(f_k^w)) \tag{10}$$

As explained in Section III, this means that the class prediction for a window is determined by the majority vote (mathematically expressed by the mode) of the class predictions made by the MLP for each individual frame within the window. This approach allows us to estimate the confidence of the prediction, which we define as:

$$\text{confidence of c(w)} = \frac{|\{f_i^w \mid c(f_i^w) = c(w)\}|}{k} \tag{11}$$

where k is the number of frames into which each window is divided. If the model predicts that window w belongs to a certain patient p_i, this confidence measure reflects the percentage of frames within w that the model assigns to that patient p_i. For example, if the confidence of a window is 0.9, it means the model predicts that 90% of its frames correspond to patient p_i, indicating a high level of confidence in the prediction. In Figure 5, we have grouped the windows into bins according to their confidence level and prediction outcome. A window is considered to have a successful prediction when the class predicted by the model matches the actual patient to whom the window belongs. Otherwise, the prediction is classified as a failure. Moreover, while observing that most windows are predicted with high confidence (64.29% of windows show a confidence level exceeding 90%), we also observe that the actual accuracy within each confidence range is higher than the estimated confidence. This suggests that the confidence values provided by the model are conservative estimates. This relationship is further illustrated in Table V, which compares the confidence estimates provided by the model (Confidence Range) with the actual prediction accuracy (Success Percentage) for the test windows. The success rate consistently exceeds the confidence estimates in all cases.

All experiments were conducted on a workstation equipped with an Intel 12th Gen Core i7-12700KF CPU and an NVIDIA

TABLE IV
PERFORMANCE METRICS FOR RESNET50 AND CUSTOMIZED CNN MODELS IN DIFFERENT SCENARIOS

	Accuracy (%)	FAR (%)	FRR (%)	Precision (%)	Recall (%)	F1-score
All scenarios						
ResNet50	89.10	10.50	10.90	89.50	89.10	0.891
Customized CNN	91.20	8.50	8.80	91.50	91.20	0.912
Resting scenario						
ResNet50	93.10	5.70	6.90	94.30	93.10	0.931
Customized CNN	95.40	3.90	4.60	96.10	95.40	0.954

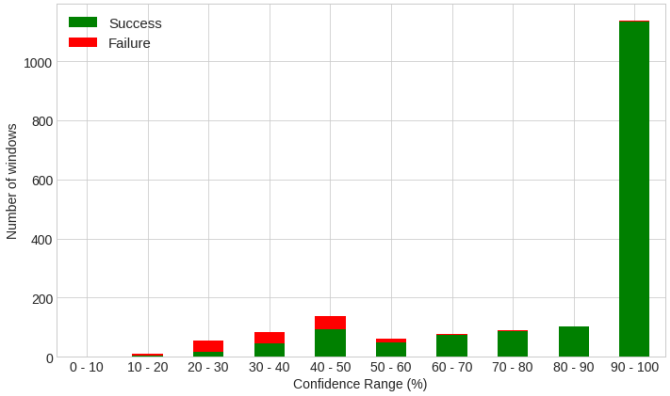

Fig. 5. Prediction confidence of windows by success

TABLE V
SUCCESS PERCENTAGE BY CONFIDENCE RANGE

Confidence Range	Success Percentage
0% - 10%	-
10% - 20%	33.33%
20% - 30%	31.34%
30% - 40%	44.93%
40% - 50%	65.69%
50% - 60%	78.08%
60% - 70%	90.24%
70% - 80%	95.24%
80% - 90%	97.09%
90% - 100%	99.91%

GeForce RTX 3080 Ti GPU with 12 GB of memory, running Ubuntu OS. The computational demands of the proposed approach are primarily associated with the model training phase, which took approximately 195 minutes, a process that is performed only once. Once the model is trained, its execution time for processing a single window is small, less than 2 seconds. This time could potentially be further reduced through algorithmic optimization or the use of additional computational resources. This efficiency makes it suitable for real-world applications, offering a continuous identification solution with minimal latency.

V. DISCUSSION

The results obtained in our study demonstrate that cancelable identification based on the contactless extraction of cardiac signals using continuous-wave radar is feasible, thus enabling a continuous user identification system. To contextualize these findings within the broader field of cancelable biometrics, Table VII provides an overview of representative ECG-based approaches. Although our method differs substantially from these works in terms of datasets, signal modalities, and experimental setups, the table highlights that the performance achieved by our radar-based approach is comparable to that of ECG-based techniques. The aim is not to present a direct comparison, but rather to illustrate the potential of contactless radar as a viable alternative for biometric identification.

In our study, accuracy exceeds 95% in two out of the five scenarios, and reaches 94.87% in another. In the remaining two scenarios—Apnea and Tilt Up—the performance is lower, with accuracies of 74.75% and 78.19%, respectively. In the case of Apnea, the recordings are shorter, and only three apneas occur, with the last one appearing in the test set. In Tilt Up, it is likely that the physiological system disruption is significant due to the heart making a greater effort to continue providing blood flow to the upper part of the body, where the brain is located, which is the organ that requires the most blood in this context. To improve the results in these two scenarios, it would likely be necessary to have more data to train the model. It should also be noted that the results in Table III were obtained using a single model that predicts identity without accounting for the scenario. It might be possible that introducing a classifier to predict the scenario or creating a different model for each scenario could improve these results. Nonetheless, the model provides a confidence estimate in the predictions that is quite conservative, as seen in Table V. That is, if we set a confidence threshold of, for example, 50%, then 97.85% of the predictions are correct, a percentage that rises to over 99% in three out of the five scenarios. These results are detailed in Table VI, which reflects the metrics for identification in windows with a confidence greater than 50%, representing 87.19% of the total windows.

These results represent, to the best of our knowledge, the first attempt to develop a cancelable identification method using non-contact radar-based cardiac signals. Since no previous results exist for cancelable identification methods using this type of signal, we have compared our results with those obtained from similar studies using ECG signals. The rationale for this comparison is grounded in recent findings demonstrating that ECG signals can be accurately reconstructed using wave radar technology [116], [117]. Some of these

TABLE VI
METRICS FOR WINDOWS WITH PREDICTED CONFIDENCE BIGGER THAN 50%

Scenario	Accuracy (%)	FAR (%)	FRR (%)	Precision (%)	Recall (%)	F1-score (%)	Windows selected (%)
Apnea	90.28	15.22	6.85	84.78	89.10	84.30	72.73
Resting	99.17	1.23	0.72	98.77	99.28	98.92	92.07
TiltDown	99.08	0.88	1.07	99.12	98.93	98.98	91.85
TiltUp	94.02	8.50	6.66	91.50	93.34	91.46	71.10
Valsalva	99.05	1.12	0.82	98.88	99.18	99.00	93.45
All	97.85	2.06	1.99	97.94	98.01	97.95	87.19

comparative results are shown in Table VII, where the "Performance" column reflects results gathered from the manuscripts of those studies. This table also includes the dataset used in each study. The Physikalisch Technische Bundesanstalt (PTB) Database provides high-resolution ECG recordings from a Frank-lead vectorcardiogram and a standard 12-lead ECG, collected under controlled conditions. The CYBHi Database is designed for cardiac biometrics, offering ECG signals sampled at 1 kHz with 12-bit resolution, recorded using dry electrodes on palms or Electrolycras on fingers. The MIT-BIH Arrhythmia Dataset features 48 two-channel recordings, each 30 minutes long, sampled at 360 Hz with 11-bit resolution, covering both normal rhythms and complex arrhythmia. Each of these datasets is affected by specific artifacts, such as baseline wander from respiration and body movement in the PTB and CYBHi databases, and electrode motion artifact in the MIT-BIH Arrhythmia Dataset [118]. In the case of [119], the authors mention the possible presence of power line interference, baseline wander, and muscle artifacts. In our dataset, RBM and respiration are the two main sources of noise, although future studies could explore the possibility of leveraging the patient's respiration to enhance the identification process. It is worth noting that in our study, we opted for temporal train-test segmentation to better approximate real-world usage scenarios, a step not always taken in all studies. Using a random split approach would have resulted in very similar windows between the train and test sets, potentially contiguous, thereby improving all metrics.

Additionally, we found that feature extraction via Transfer Learning yields satisfactory results. Among the pre-trained networks we tested, ResNet50 emerged as the best performer. However, better results can be achieved in this case by extracting features using our custom-trained network, trained exclusively on images from this dataset, as shown in Table II. This enhancement does not significantly increase training time. Subsequently, the results in this table are further improved with the introduction of a cancellation method (GRP), which generates cancelable templates by acting as a feature selector. This selection can be more intense, streamlining computational calculations and enhancing security, or less intense, resulting in a less drastic reduction in the number of features in each template. Our experiments did not observe superior performance in any case, perhaps only some instability in the results if the dimensionality reduction is strong.

With this identification system based on cancelable templates, we can ensure that the four properties mentioned in the introduction are met. Firstly, the templates are unique to this application since the system has its own method of template generation. Moreover, reusability/revocability is guaranteed due to the flexibility of GRP. In case one or several templates are compromised, another projection matrix can be randomly chosen to generate new and different templates. In such a case, the model would also need to be retrained. The process carried out with GRP also guarantees non-invertibility since it involves projecting the data into a lower-dimensional subspace, making the mapping between the original and transformed spaces non-bijective and therefore lacking an inverse. Finally, regarding performance, we can affirm that our model is not computationally inefficient when compared to other biometric identification models. On the contrary, GRP acts as a feature selection tool that can reduce the number of features extracted from each scalogram (Figure 4) without compromising results, thereby facilitating good model performance.

A limitation of the present study lies in the number of patients for which the identification method was tested—30 subjects. This limitation is shared by most studies working with signals extracted via radar, and this sample size is, in fact, larger than that of most studies to date. This is due to the scarcity of available data for this type of signal, which represents a significant bottleneck in the development of related technologies. In [12], various studies on identification using radar-based signals are summarized, five of which utilize cardiac signals. These five studies report datasets containing 4, 10, 11, 20, and 78 participants, respectively (with the latter dataset being private). The studies cited in the same article that propose identification methods based on respiratory signals extracted via radar include 3, 6, 6, 10, 10, and 20 participants. Therefore, although the present study does not provide conclusive results regarding the applicability of the method in a real-world identification scenario, it makes a significant contribution to the field by offering evidence of the feasibility of the proposed methods with a sample size larger than most previous studies, while also incorporating the innovations described in the Introduction. These results, therefore, suggest the potential for implementing a secure contactless identification system through the extraction of cardiac signals using continuous-wave radar. On the other hand, the recordings were conducted in a laboratory setting, minimizing RBM. In real-world scenarios, the presence of such movements could pose a challenge to the applicability of this technique. However, some studies have already begun exploring ways to mitigate the impact of these movements. For example, in [74] Non-negative Matrix Factorization is employed to reduce body movement interference in recordings

TABLE VII
COMPARISON OF BIOMETRIC CANCELLATION TECHNIQUES AND THEIR PERFORMANCE.

Reference	Year	Type of signal	Dataset	Cancellation Method	Other Techniques	Performance
Chen et al. [120]	2017	ECG	PTB Database (285 subjects)	Subspace collapsing	MUSIC algorithm with suppression and poll strategy	Accuracy 97.58%
Wu et al. [9]	2018	ECG	PTB Database	Signal subspace collapsing	Multiple signal classification method	Accuracy 95.23%
Kim et al. [10]	2019	ECG	ECG-ID dataset	Compressive Sensing - Generalized Likelihood Ratio Test (CS-GLRT), random permutation-based revocation process	Self-guided ECG filtering, T-wave shift model	Accuracy 93.00%
Hammad et al. [121]	2019	ECG	MIT-BIH arrhythmia dataset, PTB Database, CYBHi dataset	Improved Bio-Hash and matrix operation	Feed-Forward Neural Network for identification	Equal Error Rate (EER) 14%
Sakr et al. [122]	2022	ECG	ECG-ID dataset, PTB Database	DNA and amino acid based technique	Transfer learning for feature extraction, SVM	Accuracy 99.26% and 99.39%
El-Moneim et al. [123]	2024	ECG	ECG-ID dataset, MIT-BIH dataset	Blind signal separation and lightweight encryption	XOR operation with user-specific pattern	Accuracy 99.96% and 99.96%
Our results	2024	Heartbeats (radar)	Erlangen Hospital [68]	GRP	Continuous-wave radar, CNN, MLP	Accuracy 95.40% (resting) and 91.20% (all scenarios)

of premature infants in the neonatal intensive care unit. Other studies addressing the reduction of such signal interferences include [15] and [16].

Furthermore, this technique offers new possibilities for application in various fields, always preserving user security and privacy. For example, it could be used in continuous monitoring of the cardiac system for health purposes, providing precise data for the diagnosis and management of cardiovascular diseases, in identifying specific activities performed by an individual or in assessing the level of stress they are experiencing, offering valuable tools for personal well-being and mental health management. Additionally, this system could be integrated with other biometric modalities, creating even more robust and secure multifactor identification solutions.

VI. CONCLUSION

In this study, we developed a contactless identification system based on heart signal detection using continuous-wave radar. From this signal, by isolating the part corresponding to the heart, we generated scalograms and extracted features using a CNN. With these features, we generated a cancelable template using GRP and then classified these templates with an MLP. The results showed an accuracy of 91.20% on the combined dataset of five scenarios and 95.40% when considering only the Resting scenario. The method also provides a confidence measure in the predictions, which we can use to increase our confidence in the outputs. For example, by selecting only windows with a confidence greater than 50%, we can predict the class of 87.19% of the windows with an accuracy of 97.85%, percentages which increase notably in three of the five scenarios present in the database. The results presented in this research are very promising, and we anticipate they might pave the way for new and innovative contactless cancelable biometric systems, thereby enhancing security and privacy, improving usability, and facilitating daily identification processes for users. The primary limitation in this area of research is the current scarcity of available data, which hinders progress. Aside from this, the potential of this radar-based biometric method could be comparable to other more established methods such as ECG or face recognition.

REFERENCIES

[1] A. Jain, R. Bolle, and S. Pankanti, *Introduction to Biometrics*. Boston, MA: Springer US, 1996, pp. 1–41. [Online]. Available: https://doi.org/10.1007/0-306-47044-6_1

[2] K. Simoens, P. Tuyls, and B. Preneel, "Privacy weaknesses in biometric sketches," in *2009 30th IEEE Symposium on Security and Privacy*, 2009, pp. 188–203.

[3] "ISO/IEC 24745:2022 information technology — security techniques — biometric template protection," International Organization for Standardization, 2022, available at https://www.iso.org/standard/75302.html.

[4] M. Rawat and N. Kumar, "Cancelable biometrics: a comprehensive survey," *Artificial Intelligence Review*, vol. 53, 06 2020.

[5] S. Wang and J. Hu, "Design of alignment-free cancelable fingerprint templates via curtailed circular convolution," *Pattern Recognition*, vol. 47, no. 3, pp. 1321–1329, 2014, handwriting Recognition and other PR Applications. [Online]. Available: https://www.sciencedirect.com/science/article/pii/S0031320313004093

[6] J. K. Pillai, V. M. Patel, R. Chellappa, and N. K. Ratha, "Secure and robust iris recognition using random projections and sparse representations," *IEEE Transactions on Pattern Analysis and Machine Intelligence*, vol. 33, no. 9, p. 1877 – 1893, 2011, cited by: 256; All Open Access, Green Open Access. [Online]. Available: https://www.scopus.com/inward/record.uri?eid=2-s2.0-80054910703&doi=10.1109%2fTPAMI.2011.34&partnerID=40&md5=5d8451a6e2c122bc4794cab9ee3291d2

[7] L. Leng and J. Zhang, "Palmhash code vs. palmphasor code," *Neurocomputing*, vol. 108, pp. 1–12, 2013. [Online]. Available: https://www.sciencedirect.com/science/article/pii/S0925231212006947

[8] M. Hammad, G. Luo, and K. Wang, "Cancelable biometric authentication system based on ecg," *Multimedia Tools and Applications*, vol. 78, pp. 1857–1887, 2019.

[9] S.-C. Wu, P.-T. Chen, A. L. Swindlehurst, and P.-L. Hung, "Cancelable biometric recognition with ecgs: subspace-based approaches," *IEEE Transactions on Information Forensics and Security*, vol. 14, no. 5, pp. 1323–1336, 2018.

[10] H. Kim and S. Y. Chun, "Cancelable ecg biometrics using compressive sensing-generalized likelihood ratio test," *IEEE Access*, vol. 7, pp. 9232–9242, 2019.

[11] K. Shi, C. Will, R. Weigel, and A. Koelpin, "Contactless person identification using cardiac radar signals," in *2018 IEEE International Instrumentation and Measurement Technology Conference (I2MTC)*, 2018, pp. 1–6.

[12] S. M. M. Islam, O. Borić-Lubecke, Y. Zheng, and V. M. Lubecke, "Radar-based non-contact continuous identity authentication," *Remote Sensing*, vol. 12, no. 14, 2020. [Online]. Available: https://www.mdpi.com/2072-4292/12/14/2279

[13] H. JE, "Guyton and hall textbook of medical physiology e-book. amsterdam," *Netherlands: Elsevier Health Sciences*, 2010.

[14] I.-S. Lee and J.-R. Yang, "Signal preprocessing for heartbeat detection using continuous-wave doppler radar," *IEEE Microwave and Wireless Technology Letters*, vol. 33, no. 4, pp. 479–482, 2023.

[15] F. Zhu, K. Wang, and K. Wu, "Doppler radar techniques for vital signs detection featuring noise cancellation," in *2019 IEEE MTT-S International Microwave Biomedical Conference (IMBioC)*, vol. 1, 2019, pp. 1–4.

[16] C. Gouveia, J. Vieira, and P. Pinho, "A review on methods for random motion detection and compensation in bio-radar systems," *Sensors*, vol. 19, no. 3, p. 604, 2019.

[17] M. Sharif, M. Raza, J. H. Shah, M. Yasmin, and S. L. Fernandes, "An overview of biometrics methods," *Handbook of Multimedia Information Security: Techniques and Applications*, pp. 15–35, 2019.

[18] A. N. Uwaechia and D. A. Ramli, "A comprehensive survey on ecg signals as new biometric modality for human authentication: Recent advances and future challenges," *IEEE Access*, vol. 9, pp. 97 760–97 802, 2021.

[19] L. Biel, O. Pettersson, L. Philipson, and P. Wide, "Ecg analysis: a new approach in human identification," *IEEE Transactions on Instrumentation and Measurement*, vol. 50, no. 3, pp. 808–812, 2001.

[20] T. Wartzek, B. Eilebrecht, J. Lem, H.-J. Lindner, S. Leonhardt, and M. Walter, "Ecg on the road: Robust and unobtrusive estimation of heart rate," *IEEE Transactions on biomedical engineering*, vol. 58, no. 11, pp. 3112–3120, 2011.

[21] X. Liu, H. Wang, Z. Li, and L. Qin, "Deep learning in ecg diagnosis: A review," *Knowledge-Based Systems*, vol. 227, p. 107187, 2021.

[22] X. Zhang, M. Jiang, K. Polat, A. Alhudhaif, J. Hemanth, and W. Wu, "Detection of atrial fibrillation from variable-duration ecg signal based on time-adaptive densely network and feature enhancement strategy," *IEEE Journal of Biomedical and Health Informatics*, vol. 27, no. 2, pp. 944–955, 2023.

[23] M. Ingale, R. Cordeiro, S. Thentu, Y. Park, and N. Karimian, "Ecg biometric authentication: A comparative analysis," *IEEE Access*, vol. 8, pp. 117 853–117 866, 2020.

[24] M. Hammad, P. Pławiak, K. Wang, and U. R. Acharya, "Resnet-attention model for human authentication using ecg signals," *Expert Systems*, vol. 38, no. 6, p. e12547, 2021.

[25] E. Ihsanto, K. Ramli, D. Sudiana, and T. S. Gunawan, "Fast and accurate algorithm for ecg authentication using residual depthwise separable convolutional neural networks," *Applied Sciences*, vol. 10, no. 9, p. 3304, 2020.

[26] Y. Li, Y. Pang, K. Wang, and X. Li, "Toward improving ecg biometric identification using cascaded convolutional neural networks," *Neurocomputing*, vol. 387, pp. 72–81, 2020.

[27] D. Jyotishi and S. Dandapat, "An lstm-based model for person identification using ecg signal," *IEEE Sensors Letters*, vol. 4, no. 8, pp. 1–4, 2020.

[28] C. Fuster-Barcelo, P. Peris-Lopez, and C. Camara, "Elektra: Elektrokardiomatrix application to biometric identification with convolutional neural networks," *Neurocomputing*, vol. 506, pp. 37–49, 2022, jST Material Number: W0360A.

[29] J. P. Allam, K. K. Patro, M. Hammad, R. Tadeusiewicz, and P. Pławiak, "Baed: A secured biometric authentication system using ecg signal based on deep learning techniques," *Biomedical Signal Processing and Control*, vol. 73, p. 103283, 2022. [Online]. Available: https://doi.org/10.1016/j.bbe.2022.08.004

[30] O. Ozaltin and O. Yeniay, "A novel proposed cnn–svm architecture for ecg scalograms classification," *Soft Comput*, vol. 27, pp. 4639–4658, April 2023. [Online]. Available: https://doi.org/10.1007/s00500-022-07729-x

[31] D. Wang, Y. Si, W. Yang, G. Zhang, and T. Liu, "A novel heart rate robust method for short-term electrocardiogram biometric identification," *Applied Sciences*, vol. 9, no. 1, p. 201, 2019.

[32] C. L. P. Lim, W. L. Woo, S. S. Dlay, and B. Gao, "Heartrate-dependent heartwave biometric identification with thresholding-based gmm–hmm methodology," *IEEE Transactions on Industrial Informatics*, vol. 15, no. 1, pp. 45–53, 2018.

[33] N. Akhter, S. Tharewal, V. Kale, A. Bhalerao, and K. Kale, "Heart-based biometrics and possible use of heart rate variability in biometric recognition systems," *Advanced Computing and Systems for Security: Volume 1*, pp. 15–29, 2016.

[34] N. Akhter, S. Dabhade, N. Bansod, and K. Kale, "Feature selection for heart rate variability based biometric recognition using genetic algorithm," in *Intelligent Systems Technologies and Applications: Volume 1*. Springer, 2016, pp. 91–101.

[35] T. Hilbel and N. Frey, "Review of current ecg consumer electronics (pros and cons)," *Journal of Electrocardiology*, vol. 77, pp. 23–28, 2023.

[36] M. Liebetruth, K. Kehe, D. Steinritz, and S. Sammito, "Systematic literature review regarding heart rate and respiratory rate measurement by means of radar technology," *Sensors*, vol. 24, no. 3, p. 1003, 2024.

[37] F. Michler, K. Shi, S. Schellenberger, T. Steigleder, A. Malessa, L. Hameyer, N. Neumann, F. Lurz, C. Ostgathe, R. Weigel *et al.*, "A clinically evaluated interferometric continuous-wave radar system for the contactless measurement of human vital parameters," *Sensors*, vol. 19, no. 11, p. 2492, 2019.

[38] A. S. D. Lopes, "Bio-radar applications for remote vital signs monitoring," Master's thesis, Faculdade de Ciências e Tecnologia, Universidade Nova de Lisboa, February 2021, master's thesis, Universidade Nova de Lisboa. [Online]. Available: http://hdl.handle.net/10362/118695

[39] L. Liu, W. Xiao, J. Wu, and S. Xiao, "Wavelet analysis based noncontact vital signal measurements using mm-wave radar," in *Lecture Notes in Computer Science*, vol. 12398, 2020. [Online]. Available: https://link.springer.com/chapter/10.1007/978-3-030-64243-3_1

[40] C. Gouveia, D. Albuquerque, P. Pinho, and J. Vieira, "Evaluation of heartbeat signal extraction methods using a 5.8 ghz doppler radar system in a real application scenario," *IEEE Sensors Journal*, vol. 22, no. 8, pp. 7979–7989, 2022.

[41] F. Lin, C. Song, Y. Zhuang, W. Xu, C. Li, and K. Ren, "Cardiac scan: A non-contact and continuous heart-based user authentication system," in *Proceedings of the 23rd Annual International Conference on Mobile Computing and Networking*, ser. MobiCom '17. New York, NY, USA: Association for Computing Machinery, 2017, p. 315–328. [Online]. Available: https://doi.org/10.1145/3117811.3117839

[42] P. Cao, W. Xia, and Y. Li, "Heart id: Human identification based on radar micro-doppler signatures of the heart using deep learning," *Remote Sensing*, vol. 11, no. 10, 2019. [Online]. Available: https://www.mdpi.com/2072-4292/11/10/1220

[43] N. T. P. Van, L. Tang, A. Singh, N. D. Minh, S. C. Mukhopadhyay, and S. F. Hasan, "Self-identification respiratory disorder based on continuous wave radar sensor system," *IEEE Access*, vol. 7, pp. 40 019–40 026, 2019.

[44] M. Otero, "Application of a continuous wave radar for human gait recognition," in *Signal Processing, Sensor Fusion, and Target Recognition XIV*, vol. 5809. SPIE, 2005, pp. 538–548.

[45] M. Forouzanfar, M. Mabrouk, S. Rajan, M. Bolic, H. R. Dajani, and V. Z. Groza, "Event recognition for contactless activity monitoring using phase-modulated continuous wave radar," *IEEE Transactions on Biomedical Engineering*, vol. 64, no. 2, pp. 479–491, 2016.

[46] C. Gouveia, A. Tomé, F. Barros, S. C. Soares, J. Vieira, and P. Pinho, "Study on the usage feasibility of continuous-wave radar for emotion recognition," *Biomedical Signal Processing and Control*, vol. 58, p. 101835, 2020.

[47] J. Pegoraro, F. Meneghello, and M. Rossi, "Multiperson continuous tracking and identification from mm-wave micro-doppler signatures," *IEEE Transactions on Geoscience and Remote Sensing*, vol. 59, no. 4, pp. 2994–3009, 2020.

[48] N. Ratha, J. Connell, and R. Bolle, "Enhancing security and privacy in biometrics-based authentication systems," *IBM Systems Journal*, vol. 40, pp. 614–634, 01 2001.

[49] J. C. Bernal-Romero, J. M. Ramirez-Cortes, J. D. J. Rangel-Magdaleno, P. Gomez-Gil, H. Peregrina-Barreto, and I. Cruz-Vega, "A review on protection and cancelable techniques in biometric systems," *IEEE Access*, vol. 11, pp. 8531–8568, 2023.

[50] D. Arpit, G. Srivastava, and V. Govindaraju, "Randomized subspace learning algorithms with subspace structure preservation guarantees," *CoRR*, vol. abs/1401.4489, 2014. [Online]. Available: http://arxiv.org/abs/1401.4489

[51] A. T. B. Jin, D. N. C. Ling, and A. Goh, "Biohashing: two factor authentication featuring fingerprint data and tokenised random number," *Pattern recognition*, vol. 37, no. 11, pp. 2245–2255, 2004.

[52] A. B. Teoh and D. C. Ngo, "Random multispace quantization as an analytic mechanism for biohashing of biometric and random identity inputs," *IEEE Transactions on Pattern Analysis and Machine Intelligence*, vol. 28, no. 12, p. 1892 – 1901, 2006, cited by: 355. [Online]. Available: https://www.scopus.com/inward/record.uri?eid=2-s2.0-33947177191&doi=10.1109%2fTPAMI.2006.250&partnerID=40&md5=50b919a91bc6a94240894378d3942091

[53] A. B. J. Teoh and C. T. Yuang, "Cancelable biometrics realization with multispace random projections," *IEEE Transactions on Systems, Man, and Cybernetics, Part B: Cybernetics*, vol. 37,

no. 5, p. 1096 – 1106, 2007, cited by: 143. [Online]. Available: https://www.scopus.com/inward/record.uri?eid=2-s2.0-35148885090&doi=10.1109%2fTSMCB.2007.903538&partnerID=40&md5=250d54b50f8af30b547b479b36efdd4c

[54] A. B. J. Teoh, W.-K. Yip, and K.-A. Toh, "Cancellable biometrics and user-dependent multi-state discretization in biohash," *Pattern Analysis and Applications*, vol. 13, pp. 301–307, 8 2010.

[55] J. K. Pillai, V. M. Patel, R. Chellappa, and N. K. Ratha, "Sectored random projections for cancelable iris biometrics," in *2010 IEEE International Conference on Acoustics, Speech and Signal Processing*, 2010, pp. 1838–1841.

[56] Y. Wang and K. N. Plataniotis, "An analysis of random projection for changeable and privacy-preserving biometric verification," *IEEE Transactions on Systems, Man, and Cybernetics, Part B: Cybernetics*, vol. 40, no. 5, p. 1280 – 1293, 2010, cited by: 54. [Online]. Available: https://www.scopus.com/inward/record.uri?eid=2-s2.0-77956684084&doi=10.1109%2fTSMCB.2009.2037131&partnerID=40&md5=fbe238c2ab7593fe2d74207cc4263044

[57] B. Yang, D. Hartung, K. Simoens, and C. Busch, "Dynamic random projection for biometric template protection," in *2010 Fourth IEEE international conference on biometrics: theory, applications and systems (BTAS)*. IEEE, 2010, pp. 1–7.

[58] W. Yang, S. Wang, J. Hu, Z. Guanglou, and C. Valli, "A fingerprint and finger-vein based cancelable multi-biometric system," *Pattern Recognition*, vol. 78, 06 2018.

[59] R. Rani, R. Dhir, and K. Sonkar, "Random projection-based cancelable iris biometrics for human identification using deep learning," *Arabian Journal for Science and Engineering*, vol. 49, pp. 3815–3828, March 2024, received 31 March 2022, Accepted 24 July 2023, Published 19 August 2023, Issue Date March 2024. [Online]. Available: https://doi.org/10.1007/s13369-023-08190-0

[60] H. Djebli, S. Ait-Aoudia, and D. Michelucci, "Quantized random projections of sift features for cancelable fingerprints," *Multimedia Tools and Applications*, vol. 82, pp. 7917–7937, February 2023, received 09 November 2021, Revised 29 June 2022, Accepted 02 August 2022, Published 15 August 2022, Issue Date February 2023. [Online]. Available: https://doi.org/10.1007/s11042-022-13646-w

[61] W. Yongjin and D. Hatzinakos, "Sorted index numbers for privacy preserving face recognition," *EURASIP Journal on Advances in Signal Processing*, vol. 2009, 12 2009.

[62] M. Deshmukh and M. K. Balwant, "Generating cancelable palmprint templates using local binary pattern and random projection," in *2017 13th International Conference on Signal-Image Technology Internet-Based Systems (SITIS)*, 2017, pp. 203–209.

[63] M. Dey, N. Dey, S. Mahata, S. Chakraborty, S. Acharjee, and A. Das, "Electrocardiogram feature based inter-human biometric authentication system," 01 2014, pp. 300–304.

[64] H. Kim and S. Y. Chun, "Cancelable ecg biometrics using compressive sensing-generalized likelihood ratio test," *IEEE Access*, vol. 7, pp. 9232–9242, 2019.

[65] P.-T. Chen, S.-C. Wu, and J.-H. Hsieh, "A cancelable biometric scheme based on multi-lead ecgs," in *2017 39th Annual International Conference of the IEEE Engineering in Medicine and Biology Society (EMBC)*, 2017, pp. 3497–3500.

[66] S. Eldesouky, W. El-Shafai, H. E. d. H. Ahmed, and F. E. A. El-Samie, "Cancelable electrocardiogram biometric system based on chaotic encryption using three-dimensional logistic map for biometric-based cloud services," *SECURITY AND PRIVACY*, vol. 5, no. 2, p. e198, 2022. [Online]. Available: https://onlinelibrary.wiley.com/doi/abs/10.1002/spy2.198

[67] E.-M. Kabel, G. El-Banby, and L. e. a. Abou Elazm, "Securing internet-of-medical-things networks using cancellable ecg recognition," *Scientific Reports*, vol. 14, p. 10871, 2024. [Online]. Available: https://doi.org/10.1038/s41598-024-54830-2

[68] S. Chellenberger, K. Shi, T. Steigleder *et al.*, "A dataset of clinically recorded radar vital signs with synchronised reference sensor signals," *Sci Data*, vol. 7, p. 291, 2020. [Online]. Available: https://doi.org/10.1038/s41597-020-00629-5

[69] ——, "A dataset of clinically recorded radar vital signs with synchronised reference sensor signals," https://figshare.com/articles/dataset/A_dataset_of_clinically_recorded_radar_vital_signs_with_synchronised_reference_sensor_signals/12186516, 2020.

[70] B. Yan, H. Zhang, Y. Yao, C. Liu, P. Jian, P. Wang, L. Du, X. Chen, Z. Fang, and Y. Wu, "Heart signatures: Open-set person identification based on cardiac radar signals," *Biomedical Signal Processing and Control*, vol. 72, p. 103306, 2022. [Online]. Available: https://www.sciencedirect.com/science/article/pii/S1746809421009034

[71] A. Alkasimi, T. Shepard, S. Wagner, S. Pancrazio, A.-V. Pham, C. Gardner, and B. Funsten, "Dual-biometric human identification using radar deep transfer learning," *Sensors*, vol. 22, no. 15, 2022. [Online]. Available: https://www.mdpi.com/1424-8220/22/15/5782

[72] H. J. Lee, H. S. Kim, and K. S. Park, "A study on the reproducibility of biometric authentication based on electroencephalogram (eeg)," in *2013 6th International IEEE/EMBS Conference on Neural Engineering (NER)*, 2013, pp. 13–16.

[73] F.-K. Wang, J.-X. Zhong, and J.-Y. Shih, "Iq signal demodulation for noncontact vital sign monitoring using a cw doppler radar: A review," *IEEE Journal of Electromagnetics, RF and Microwaves in Medicine and Biology*, vol. 6, no. 4, pp. 449–460, 2022.

[74] G. Beltrão, R. Stutz, F. Hornberger *et al.*, "Contactless radar-based breathing monitoring of premature infants in the neonatal intensive care unit," *Scientific Reports*, vol. 12, p. 5150, 2022. [Online]. Available: https://doi.org/10.1038/s41598-022-08836-3

[75] M. Zakrzewski, A. Singh, E. Yavari, X. Gao, O. Boric-Lubecke, J. Vanhala, and K. Palovuori, "Quadrature imbalance compensation with ellipse-fitting methods for microwave radar physiological sensing," *IEEE Transactions on Microwave Theory and Techniques*, vol. 62, no. 6, pp. 1400–1408, 2014.

[76] B.-K. Park, O. Boric-Lubecke, and V. M. Lubecke, "Arctangent demodulation with dc offset compensation in quadrature doppler radar receiver systems," *IEEE Transactions on Microwave Theory and Techniques*, vol. 55, no. 5, pp. 1073–1079, 2007.

[77] C. Gouveia, D. Albuquerque, P. Pinho, and J. Vieira, "Evaluation of heartbeat signal extraction methods using a 5.8 ghz doppler radar system in a real application scenario," *IEEE Sensors Journal*, vol. 22, no. 8, pp. 7979–7989, 2022.

[78] S. Mallat, *A wavelet tour of signal processing*. Elsevier, 1999.

[79] G. R. Garcia, G. Michau, M. Ducoffe, J. S. Gupta, and O. Fink, "Time series to images: Monitoring the condition of industrial assets with deep learning image processing algorithms," *arXiv preprint arXiv:2005.07031*, 2020.

[80] Y.-H. Byeon, S.-B. Pan, and K.-C. Kwak, "Intelligent deep models based on scalograms of electrocardiogram signals for biometrics," *Sensors*, vol. 19, no. 4, 2019. [Online]. Available: https://www.mdpi.com/1424-8220/19/4/935

[81] A. Narin, "Detection of focal and non-focal epileptic seizure using continuous wavelet transform-based scalogram images and pre-trained deep neural networks," *Irbm*, vol. 43, no. 1, pp. 22–31, 2022.

[82] E. Benmalek, J. Elmhamdi, and A. Jilbab, "Ecg scalogram classification with cnn micro-architectures," *Research on Biomedical Engineering*, pp. 1–11, 2022.

[83] K. Kumar, K. Gupta, M. Sharma, V. Bajaj, and U. Rajendra Acharya, "Insomnet: Automated insomnia detection using scalogram and deep neural networks with ecg signals," *Medical Engineering Physics*, vol. 119, p. 104028, 2023. [Online]. Available: https://www.sciencedirect.com/science/article/pii/S1350453323000838

[84] F. R. Mashrur, M. S. Islam, D. K. Saha, S. R. Islam, and M. A. Moni, "Scnn: Scalogram-based convolutional neural network to detect obstructive sleep apnea using single-lead electrocardiogram signals," *Computers in Biology and Medicine*, vol. 134, p. 104532, 2021. [Online]. Available: https://www.sciencedirect.com/science/article/pii/S0010482521003267

[85] C. K. Chui, *An introduction to wavelets*. Elsevier, 2016.

[86] M. Jogin, Mohana, M. S. Madhulika, G. D. Divya, R. K. Meghana, and S. Apoorva, "Feature extraction using convolution neural networks (cnn) and deep learning," in *2018 3rd IEEE International Conference on Recent Trends in Electronics, Information Communication Technology (RTEICT)*, 2018, pp. 2319–2323.

[87] Z. Wan, R. Yang, M. Huang, N. Zeng, and X. Liu, "A review on transfer learning in eeg signal analysis," *Neurocomputing*, vol. 421, pp. 1–14, 2021.

[88] E. B. Mazomenos, D. Biswas, A. Acharyya, T. Chen, K. Maharatna, J. Rosengarten, J. M. Morgan, and N. Curzen, "A low-complexity ecg feature extraction algorithm for mobile healthcare applications," *IEEE Journal of Biomedical and Health Informatics*, vol. 17, pp. 459–469, 2013. [Online]. Available: https://api.semanticscholar.org/CorpusID:264233899

[89] H. E. Kim, A. Cosa-Linan, N. Santhanam, M. Jannesari, M. E. Maros, and T. Ganslandt, "Transfer learning for medical image classification: a literature review," *BMC medical imaging*, vol. 22, no. 1, p. 69, 2022.

[90] L. Torrey and J. Shavlik, "Transfer learning," in *Handbook of research on machine learning applications and trends: algorithms, methods, and techniques*. IGI global, 2010, pp. 242–264.

[91] M. A. Morid, A. Borjali, and G. Del Fiol, "A scoping review of transfer learning research on medical image analysis using imagenet," *Computers in biology and medicine*, vol. 128, p. 104115, 2021.

[92] M. K. Gajendran, M. Z. Khan, and M. A. K. Khattak, "Ecg classification using deep transfer learning," in *2021 4th International Conference on Information and Computer Technologies (ICICT)*, 2021, pp. 1–5.

[93] S. Ismail, B. Ismail, I. Siddiqi, and U. Akram, "Pcg classification through spectrogram using transfer learning," *Biomedical Signal Processing and Control*, vol. 79, p. 104075, 2023. [Online]. Available: https://www.sciencedirect.com/science/article/pii/S1746809422005407

[94] K. N. Khan, F. A. Khan, A. Abid, T. Olmez, Z. Dokur, A. Khandakar, M. E. Chowdhury, and M. S. Khan, "Deep learning based classification of unsegmented phonocardiogram spectrograms leveraging transfer learning," *Physiological measurement*, vol. 42, no. 9, p. 095003, 2021.

[95] S. Padi, S. O. Sadjadi, R. D. Sriram, and D. Manocha, "Improved speech emotion recognition using transfer learning and spectrogram augmentation," in *Proceedings of the 2021 international conference on multimodal interaction*, 2021, pp. 645–652.

[96] K. W. Gunawan, A. A. Hidayat, T. W. Cenggoro, and B. Pardamean, "A transfer learning strategy for owl sound classification by using image classification model with audio spectrogram," *International Journal on Electrical Engineering and Informatics*, vol. 13, no. 3, pp. 546–553, 2021.

[97] P. Sharma, H. Amhia, and S. D. Sharma, "Transfer learning-based model for rolling bearing fault classification using cwt-based scalograms," in *Proceedings of Third International Conference on Intelligent Computing, Information and Control Systems: ICICCS 2021*. Springer, 2022, pp. 565–576.

[98] K. He, X. Zhang, S. Ren, and J. Sun, "Deep residual learning for image recognition," in *Proceedings of the IEEE conference on computer vision and pattern recognition*, 2016, pp. 770–778.

[99] G. Huang, Z. Liu, L. Van Der Maaten, and K. Q. Weinberger, "Densely connected convolutional networks," in *Proceedings of the IEEE conference on computer vision and pattern recognition*, 2017, pp. 4700–4708.

[100] X. Zhang, X. Zhou, M. Lin, and J. Sun, "Shufflenet: An extremely efficient convolutional neural network for mobile devices," in *Proceedings of the IEEE conference on computer vision and pattern recognition*, 2018, pp. 6848–6856.

[101] K. Simonyan and A. Zisserman, "Very deep convolutional networks for large-scale image recognition," *arXiv preprint arXiv:1409.1556*, 2014.

[102] F. Chollet, "Xception: Deep learning with depthwise separable convolutions," in *Proceedings of the IEEE conference on computer vision and pattern recognition*, 2017, pp. 1251–1258.

[103] L. Torrey and J. Shavlik, "Transfer learning," in *Handbook of research on machine learning applications and trends: algorithms, methods, and techniques*. IGI global, 2010, pp. 242–264.

[104] S. Santurkar, D. Tsipras, A. Ilyas, and A. Madry, "How does batch normalization help optimization?" *Advances in neural information processing systems*, vol. 31, 2018.

[105] E. Bingham and H. Mannila, "Random projection in dimensionality reduction: applications to image and text data," in *Proceedings of the seventh ACM SIGKDD international conference on Knowledge discovery and data mining*, 2001, pp. 245–250.

[106] S. Venkatasubramanian and Q. Wang, *The Johnson-Lindenstrauss Transform: An Empirical Study*, pp. 164–173. [Online]. Available: https://epubs.siam.org/doi/abs/10.1137/1.9781611972917.16

[107] A. B. Teoh, Y. W. Kuan, and S. Lee, "Cancellable biometrics and annotations on biohash," *Pattern Recognition*, vol. 41, no. 6, pp. 2034–2044, 2008. [Online]. Available: https://www.sciencedirect.com/science/article/pii/S0031320307005298

[108] J. Deng, W. Dong, R. Socher, L.-J. Li, K. Li, and L. Fei-Fei, "Imagenet: A large-scale hierarchical image database," in *2009 IEEE Conference on Computer Vision and Pattern Recognition*, 2009, pp. 248–255.

[109] M. Grandini, E. Bagli, and G. Visani, "Metrics for multi-class classification: an overview," *arXiv preprint arXiv:2008.05756*, 2020.

[110] Z. Zhao, L. Alzubaidi, J. Zhang, Y. Duan, and Y. Gu, "A comparison review of transfer learning and self-supervised learning: Definitions, applications, advantages and limitations," *Expert Systems with Applications*, vol. 242, p. 122807, 2024. [Online]. Available: https://www.sciencedirect.com/science/article/pii/S0957417423033092

[111] S. Woo, J. Park, J.-Y. Lee, and I. S. Kweon, "Cbam: Convolutional block attention module," in *Proceedings of the European conference on computer vision (ECCV)*, 2018, pp. 3–19.

[112] K. Ma, A. Z. Chang'an, and F. Yang, "Multi-classification of arrhythmias using resnet with cbam on cwgan-gp augmented ecg gramian angular summation field," *Biomedical Signal Processing and Control*, vol. 77, p. 103684, 2022.

[113] H. Wang, Z. Luo, J. W. Yip, C. Ye, and M. Zhang, "Ecggan: A framework for effective and interpretable electrocardiogram anomaly detection," in *Proceedings of the 29th ACM SIGKDD Conference on Knowledge Discovery and Data Mining*, 2023, pp. 5071–5081.

[114] C. Fuster-Barceló, A. Guerrero-López, C. Camara, and P. Peris-Lopez, "Exploring the power of photoplethysmogram matrix for atrial fibrillation detection with integrated explainability," *Engineering Applications of Artificial Intelligence*, vol. 133, p. 108325, 2024.

[115] C. Zednik, "Solving the black box problem: A normative framework for explainable artificial intelligence," *Philosophy & technology*, vol. 34, no. 2, pp. 265–288, 2021.

[116] Y. Zhang, R. Guan, L. Li, R. Yang, Y. Yue, and E. G. Lim, "radarode: An ode-embedded deep learning model for contactless ecg reconstruction from millimeter-wave radar," 2024. [Online]. Available: https://arxiv.org/abs/2408.01672

[117] D. Yu, M. Bouazizi, and T. Ohtsukil, "Improving heart rate range classification using doppler radar with gan-based data augmentation," in *GLOBECOM 2023-2023 IEEE Global Communications Conference*. IEEE, 2023, pp. 3885–3890.

[118] G. B. Moody and R. G. Mark, "The mit-bih arrhythmia database on cd-rom and software for use with it," in *[1990] Proceedings Computers in Cardiology*. IEEE, 1990, pp. 185–188.

[119] A. I. Siam, W. El-Shafai, L. A. Abou Elazm, N. A. El-Bahnasawy, F. E. Abd El-Samie, A. Abou Elazm, and G. M. El-Banby, "Enhanced user verification in iot applications: a fusion-based multimodal cancelable biometric system with ecg and ppg signals," *Neural Computing and Applications*, vol. 36, no. 12, pp. 6575–6595, 2024.

[120] P.-T. Chen, S.-C. Wu, and J.-H. Hsieh, "A cancelable biometric scheme based on multi-lead ecgs," in *2017 39th Annual International Conference of the IEEE Engineering in Medicine and Biology Society (EMBC)*. IEEE, 2017, pp. 3497–3500.

[121] M. Hammad, G. Luo, and K. Wang, "Cancelable biometric authentication system based on ecg," *Multimedia Tools and Applications*, vol. 78, 01 2019.

[122] A. Sakr, P. Pławiak, R. Tadeusiewicz, and M. Hammad, "Cancelable ecg biometric based on combination of deep transfer learning with dna and amino acid approaches for human authentication," *Information Sciences*, vol. 585, pp. 127–143, 03 2022.

[123] S. A. El-Moneim Kabel, G. M. El-Banby, L. A. Abou Elazm, W. El-Shafai, N. A. El-Bahnasawy, F. E. A. El-Samie, A. A. Elazm, A. I. Siam, and M. A. Abdelhamed, "Securing internet-of-medical-things networks using cancellable ecg recognition," *Scientific Reports*, vol. 14, no. 1, p. 10871, 2024.